Journal of Inorganic Biochemistry 250 (2024) 112387

Contents lists available at ScienceDirect

Journal of Inorganic Biochemistry

journal homepage: www.elsevier.com/locate/jinorgbio

Nitrobindin *versus* myoglobin: A comparative structural and functional study

Giovanna De Simone [a], Alessandra di Masi [a], Andrea Pasquadibisceglie [a], Andrea Coletta [b], Federico Sebastiani [c], Giulietta Smulevich [c], Massimo Coletta [d,*], Paolo Ascenzi [e,**]

[a] *Dipartimento di Scienze, Università Roma Tre, 00146 Roma, Italy*
[b] *Claviate, Aarhus, Denmark*
[c] *Dipartimento di Chimica "Ugo Schiff" (DICUS), Università di Firenze, 50019 Sesto Fiorentino, FI, Italy*
[d] *IRCCS Fondazione Bietti, Roma, Italy*
[e] *Laboratorio Interdipartimentale di Microscopia Elettronica, Università Roma Tre, 00146 Roma, Italy*

ARTICLE INFO

Keywords:
Nitrobindin
Myoglobin
Structure
Function
Spectroscopic properties
RNS and ROS detoxification

ABSTRACT

Most hemoproteins display an all-α-helical fold, showing the classical three on three (3/3) globin structural arrangement characterized by seven or eight α-helical segments that form a sandwich around the heme. Over the last decade, a completely distinct class of heme-proteins called nitrobindins (Nbs), which display an all-β-barrel fold, has been identified and characterized from both structural and functional perspectives. Nbs are ten-stranded anti-parallel all-β-barrel heme-proteins found across the evolutionary ladder, from bacteria to *Homo sapiens*. Myoglobin (Mb), commonly regarded as the prototype of monomeric all-α-helical globins, is involved along with the oligomeric hemoglobin (Hb) in diatomic gas transport, storage, and sensing, as well as in the detoxification of reactive nitrogen and oxygen species. On the other hand, the function(s) of Nbs is still obscure, even though it has been postulated that they might participate to O_2/NO signaling and metabolism. This function might be of the utmost importance in poorly oxygenated tissues, such as the eye's retina, where a delicate balance between oxygenation and blood flow (regulated by NO) is crucial. Dysfunction in this balance is associated with several pathological conditions, such as glaucoma and diabetic retinopathy. Here a detailed comparison of the structural, spectroscopic, and functional properties of Mb and Nbs is reported to shed light on the similarities and differences between all-α-helical and all-β-barrel heme-proteins.

1. Introduction

Most living organisms synthesize heme-proteins that perform fundamental biological functions including respiration, ligand sensing, transport, and storage, and metal-based catalysis [1–12]. According to the literature, the globin portion of heme-proteins can adopt either an all-α-helical or an all-β-barrel fold [1,2,13–15].

Myoglobin (Mb) and hemoglobin (Hb) are generally considered the prototypical all-α-helical globins. They show the classical three on three (3/3) globin fold characterized by seven or eight α-helical segments that form a sandwich around the heme [1–12,15–18]. The heme distal region is composed of helices A, B, and E, while helices F, G, and H form the heme proximal side. Although helices C and D are very short (when present), recent reports suggest their importance in modulating heme

Abbreviations: At-, *Arabidopsis thaliana*; *At*-Nb(II), ferrous *Arabidopsis thaliana* Nb; *At*-Nb(II)-CO, carbonylated *At*-Nb(II); *At*-Nb(II)-NO, nitrosylated *At*-Nb(II); *At*-Nb(III), ferric *At*-Nb; *At*-Nb(III)-NO, nitrosylated *At*-Nb(III); *Efc*-Mb(II), ferrous *Efc*-Mb; *Efc*-Mb(II)-CO, carbonylated *Efc*-Nb(II); *Efc*-Mb(II)-NO, nitrosylated *Efc*-Mb (II); *Efc*-Mb(III), ferric *Efc*-Mb; *Efc*-Mb, *Equus ferus caballus* Mb; *Efc*-Nb(III)-NO, nitrosylated *Efc*-Mb(III); EPR, spectra electron paramagnetic resonance spectra; *Hs-*, *Homo sapiens*; *Hs*-Nb(II), ferrous *Hs*-Nb; *Hs*-Nb(II)-CO, carbonylated *Hs*-Nb(II); *Hs*-Nb(II)-NO, nitrosylated *Hs*-Nb(II); *Hs*-Nb(III), ferric *Hs*-Nb; *Hs*-Nb(III)-NO, nitrosylated *Hs*-Nb(III); Mb, myoglobin; *Mt-*, *Mycobacterium tuberculosis*; *Mt*-Nb(II), ferrous *Mt*-Nb; *Mt*-Nb(II)-CO, carbonylated *Mt*-Nb(II); *Mt*-Nb(II)-NO, nitrosylated *Mt*-Nb(II); *Mt*-Nb(III), ferric *Mt*-Nb; *Mt*-Nb(III)-NO, nitrosylated *Mt*-Nb(III); Nb, nitrobindin; Nb(II), ferrous Nb; Nb(II)-CO, carbonylated Nb(II); Nb(II)-NO, nitrosylated Nb(II); Nb(III), ferric Nb; Nb(III)-NO, nitrosylated Nb(III); *Pc*-Mb(II), ferrous *Pc*-Mb; *Pc*-Mb(II)-CO, carbonylated *Pc*-Nb(II); *Pc*-Mb(II)-NO, nitrosylated *Pc*-Mb(II); *Pc*-Mb(III), ferric *Pc*-Mb; *Pc*-Mb, *Physeter catodon* Mb; *Pc*-Nb(III)-NO, nitrosylated *Pc*-Mb(III); RR, Resonance Raman; UV-Vis spectra, UV-Visible spectra.

* Correspondence to: M. Coletta, IRCCS Fondazione Bietti, Roma, Italy.
** Correspondence to: P. Ascenzi, Department of Sciences, Roma Tre University, Roma, Italy.
E-mail addresses: massimiliano.coletta@fondazionebietti.it (M. Coletta), paolo.ascenzi@uniroma3.it (P. Ascenzi).

https://doi.org/10.1016/j.jinorgbio.2023.112387
Received 12 April 2023; Received in revised form 20 September 2023; Accepted 24 September 2023
Available online 1 October 2023

reactivity [1,2,9,12,15,18–21]. In all-α-helical globins, the fifth coordination site of the heme-Fe is represented by the so-called "proximal" HisF8 residue, while the "distal" E7 residue, typically His, faces the sixth axial position of the heme-Fe-atom. The HisE7 residue contributes to stabilizing the heme-bound ligand and modulates ligand entry and dissociation by acting as a gate [2,7,12,22–24]. Interestingly, in some heme-proteins including plant 3/3 non-symbiotic Hb, two-by-two (2/2) globins, cytoglobin, and neuroglobin, the HisE7 residue may serve as the sixth coordination ligand for the heme-Fe-atom. In such cases, ligand binding is only permitted upon dissociation of the sixth-coordinating residue, resulting in a transient five-coordination state of the heme-Fe-atom [2,7,12,22–25]. The presence of a wide variety of all-α-helical heme-proteins in the all kingdoms of life has raised questions regarding their potential functions [26,27] including sensing, transport and detoxification of O_2, CO and/or NO, as well as related reactive species [1,26–29].

In the past two decades, all-β-barrel heme-proteins, including nitrobindins (Nbs) and nitrophorins (NPs) [13–15,30–36], have been identified and functionally and structurally characterized. Nbs are ten-stranded anti-parallel all-β-barrel heme-proteins present along the evolutionary ladder, from bacteria to *Homo sapiens*, as also reported for all-α-helical heme-proteins [30–33]. In Nbs, the proximal His residue serves as the fifth coordinating ligand to the heme-Fe atom, whereas the His residue facing the distal side of the heme in most all-α-helical heme-proteins is absent, preventing heme-Fe atom hexacoordination. Moreover, the high solvent exposure of the heme in NPs and Nbs prevents the redox cycle of the heme Fe-atom, which in air only exists in the ferric form unless a reducing agent, such as sodium dithionite, is employed to remove O_2 and reduce the metal center. This characteristic underlies the selective binding of small neutral and anionic molecules, such as NO [30–33,37,38].

To date, the function(s) of Nbs remains unclear, although it has been postulated that they participate in NO signaling and metabolism. Specifically, NO facilitates the anaerobic reduction of the heme-Fe(III)-atom resulting in the nitrosylation of the metal center (Nb(II)-NO) through an OH^--dependent reaction involving the transient formation of the Nb-heme-Fe(III)-NO complex [36,39]. Furthermore, Nbs catalyze the isomerization of peroxynitrite to NO_3^- and NO_2^-, in the absence or presence of CO_2 [33–35,40,41]. Lastly, Nb(II)-NO acts as an O_2 scavenger, leading to the formation of NO_3^- and Nb(III) through the transient formation of the Nb-heme-Fe(III)-NO(*O*)O adduct [35,36,39,42]. Interestingly, *Homo sapiens* Nb (*Hs*-Nb) corresponds to the *C*-terminal domain of the single-chain nuclear protein THAP4, which is 567 amino acids long. *Hs*—Nb could potentially function as a NO sensor by modulating THAP4 transcriptional function residing at its *N*-terminal modified zinc finger domain [15,31,33].

Here, the structural, spectroscopic, and functional properties of all-β-barrell Nbs are examined and compared with those of all-α-helical Mb, which is generally considered as the prototype of monomeric globins. To ensure a consistent comparison, the UV–Vis electronic absorption and resonance Raman (RR) spectra of ferric Arabidopsis thaliana Nb (*At*-Nb (III)), ferrous At-Nb (*At*-Nb(II)) and carbonylated At-Nb(II) (*At*-Nb(II)-CO) were recorded. Additionally, the kinetics of the reductive nitrosylation of *At*-Nb(III) were investigated and reported in the Supplementary Materials.

2. Structural aspects

2.1. Three-dimensional structure of Nbs

The Protein Data Bank (PDB) contains the three-dimensional structures of *Mycobacterium tuberculosis* Nb (*Mt*—Nb) (PDB ID: 6R3Y; 6R3W) [33], *Arabidopsis thaliana* Nb (*At*—Nb) (PDB ID: 3EMM) [30], *Hs*—Nb (PDB ID: 3IA8) [31]. Interestingly, all the three-dimensional structures of Nbs show a close similarity each other. The main structural differences between *Mt*—Nb [33] and *At*—Nb [30] occur at the exposed residues of the β7-β8 inter-strand loop, where *At*—Nb lack six residues compared to *Mt*—Nb. This deviation may also be associated with a marked bulging of the β7 strand in *Mt*—Nb at residues Arg111-Asp113. Ongoing computer simulation studies suggest that hydration of this region may contribute to the loss of part of the secondary structure of the β7 strand in *Mt*—Nb, leading to a higher solvent exposure of the heme. Similarly, alterations in the loop have been also observed in the structural comparison with *Hs*—Nb, with the greatest structural deviation from *Mt*—Nb occurring at the β6-β7 inter-strand loop, located at the opposite end of the barrel [31,33]. The positions of the heme-Fe atom in the three protein structures are within a 0.85 Å match [33].

Overall, the β-barrel of Nbs can be divided into three sections: (*i*) the hydrophobic heme-binding pocket, (*ii*) the central region characterized by a series of inter-strand electrostatic contacts, and (*iii*) the protein extremity in which the β-barrel is stabilized by the formation of a hydrophobic core closed to the solvent by the *N*-terminal 3_{10} α-helix [15,30–33].

The heme pocket of Nbs is relatively open, exposing the heme to the solvent, which interacts with the protein moiety through multiple van der Waals interactions. In *At*—Nb the His158 residue represents the proximal fifth coordination ligand of the metal center. Although the distal His76 side chain faces the heme on the opposite side, it is located too far away from the heme-Fe atom to properly coordinate it (Fig. 1) [15,30–33]. Notably, in *Mt*—Nb, the heme group is rotated by 180° around the direction of the methinic CHA-CHC atoms compared to *At*—Nb and *Hs*—Nb [30,31,33]. In *Mt*-Nb(III)-H_2O and *Mt*-Nb(III)-cyanide derivatives, the heme-Fe atom is in the heme plane and is coordinated to the proximal residue His155. Both the water molecule and cyanide are located at the heme distal side and they are not stabilized by any interaction with protein residues or water solvent molecules [33].

The central part of the β-barrel of Nbs shows a large inner cavity positioned below the heme group. This cavity is lined with several polar residues (*e.g.*, Glu67, His85, Glu91, Glu93, His95, Arg130 in *Mt*—Nb), which stabilize some water molecules. The cavity part located further from the heme, deeper in the protein core, is instead lined with large apolar residues [32,33].

As reported for *At*—Nb, the *N*-terminal 3_{10} helix fold is stabilized by hydrogen bonds established between the Trp30 side chain and the backbone carbonyl group of Leu26, and between the Lys165 side chain and the carbonyl groups of Leu27 and Tyr25. Almost strict conservation or conservative substitution of these key residues is observed in all the Nbs [32].

2.2. Comparison between Mb and Nbs

The different reactivity of heme-proteins depends on several factors, including the amino acid environment, solvent exposure, and positioning of the heme group within the protein structure [43]. In Mb, similar to all-α-helical hemoproteins, the heme is buried within the protein matrix and interacts with hydrophobic residues that prevent the oxidation of the heme-Fe(II) atom in Mb [2,7,10,12,44–46]. The side chain of the proximal HisF8 residue (*i.e.*, His93) represents the fifth coordination ligand of the heme-Fe atom [2,7,12,46], whereas the E7 residue (mostly His and Tyr) acts as the distal ligand of the heme-Fe atom contributing to the modulation of iron reactivity and to the stability of the heme-bound ligand (Fig. 1) [1,2,5,7,10,23,24,46–48]. In contrast, in the 10-stranded anti-parallel β-barrel of Nbs, the heme is highly exposed to the solvent, and the polar amino acid, which faces the heme distal side in most of all-α-helical heme-proteins, is absent, preventing the heme-Fe-atom hexacoordination [30–35]. The highly solvent exposed heme-Fe-atom: (*i*) is at the root of the fast auto-oxidation rate of Nbs, which is 10^4–10^5 times higher than that of mammalian globins [30,34], and (*ii*) makes the metal more accessible to ligands than Mbs [41]. In fact, while in Mbs the distal His residue blocks ligand access to the heme-Fe-atom, in Nbs the cavity on the distal side of the heme (volume ~ 600 $Å^3$) makes the metal center directly accessible to external

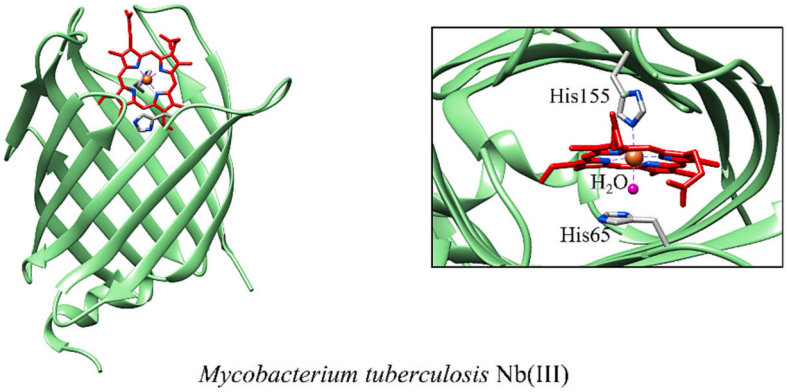

Mycobacterium tuberculosis Nb(III)

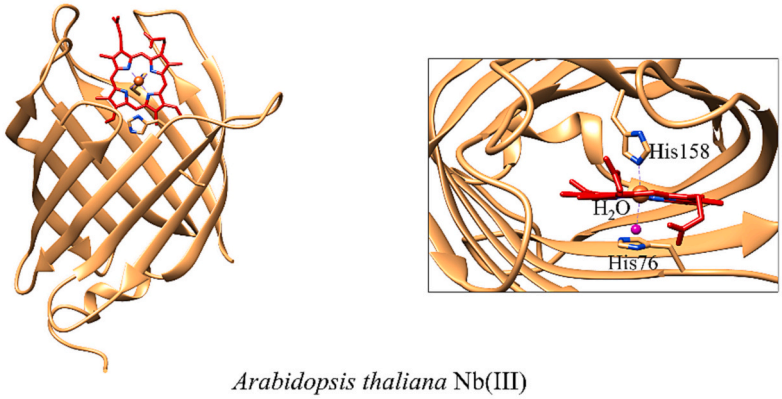

Arabidopsis thaliana Nb(III)

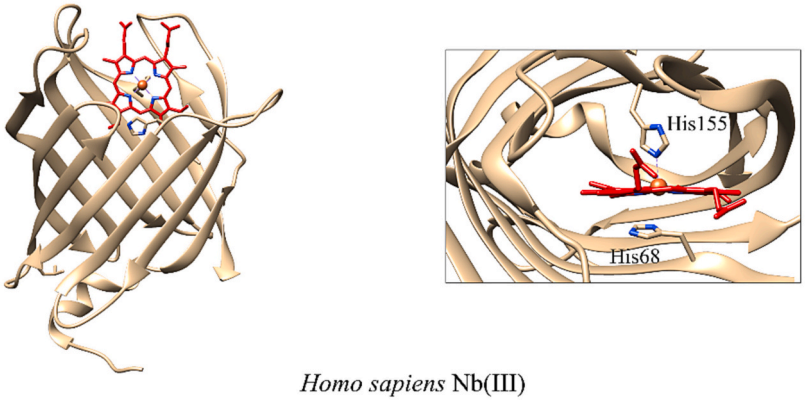

Homo sapiens Nb(III)

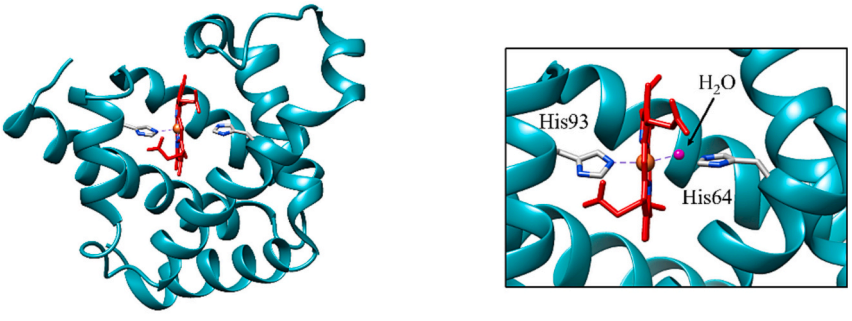

Equus ferus caballus Mb(III)

Fig. 1. Heme-pocket overview of *Mt*-Nb(III) (PDB ID: 3IA8) [33], *At*-Nb(III) (PDB ID: 3EMM) [30], *Hs*-Nb(III) (PDB ID: 3IA8) [31], and *Efc*-Mb (PDB ID: 1YMB) [93]. Proximal and distal His residues are shown in stick representation. The water coordinating molecule is colored in magenta. Figures have been drawn with UCSF-Chimera package [94]. (For interpretation of the references to colour in this figure legend, the reader is referred to the web version of this article).

ligands (Fig. 1) [2,30,31,33,41].

3. UV–visible, RR, and EPR spectroscopy

Resonance Raman (RR) spectroscopy provides a mean to investigate the structure-function relationship in heme proteins with distinct physiological functions and structural differences. In combination with UV–Vis electronic absorption spectroscopy, RR enables the examination of the heme active site within heme-proteins. RR allows the monitoring of the ligation and spin state of the heme-Fe atom and provides insights into the influence of the protein environment surrounding the metal center [49–51].

3.1. Fe(III) forms

The UV–Vis electronic absorption spectra of ferric Nb (Nbs(III)) are characteristic of High Spin (HS) species. In agreement with the UV–Vis electronic absorption spectroscopy (Fig. 2, panel A), the RR core size marker bands of ferric *Mt*-Nb, *At*-Nb, and Hs-Nb (*i.e.*, *Mt*-Nb(III), *At*-Nb(III), and *Hs*-Nb(III), respectively) at pH 6.0 (Fig. 2, panel B) are indicative of a predominant hexacoordinated high spin (6cHS) His-Fe-H_2O species [33], similarly to ferric *Equus ferus caballus* Mb (*Efc*-Mb(III)) [43,52]. For *Mt*-Nb (III), an additional penta-coordinated high spin (5cHS) species was observed. At higher pH (data not shown), an hexacoordinated low spin (6cLS) population was also detected (ν_2 at 1506/1508 cm^{-1} and ν_{10} at 1640 cm^{-1}) for *Mt*-Nb(III) and assigned to a His-Fe-OH^- species [33].

The RR spectra in the high wavenumber region (Fig. 2, panel B) also show the presence of the ν(C=C) vinyl stretching modes. The vinyl stretching modes give rise to a single band at 1621–1623 cm^{-1} in *Mt*-Nb (III) [33] and *At*-Nb(III), indicating that the two vinyl groups have very similar orientation and, as in *Efc*-Mb(III) [43,52], are almost coplanar (in "*trans*" configuration [53]), with a high degree of conjugation. Conversely, in *Hs*-Nb(III) [33], the ν(C=C) modes are found at 1623 and 1629 cm^{-1}, respectively, highlighting that the two vinyl groups are characterized by different orientations with respect to porphyrin double bonds ($C_a = C_b$), with one vinyl being less conjugated.

In the low frequency RR spectra (Fig. 2, panel B), the $\delta(C_\beta C_a C_b)$ vinyl bending modes of the ferric *Mt*-Nb(III) and *Hs*-Nb(III) are very similar

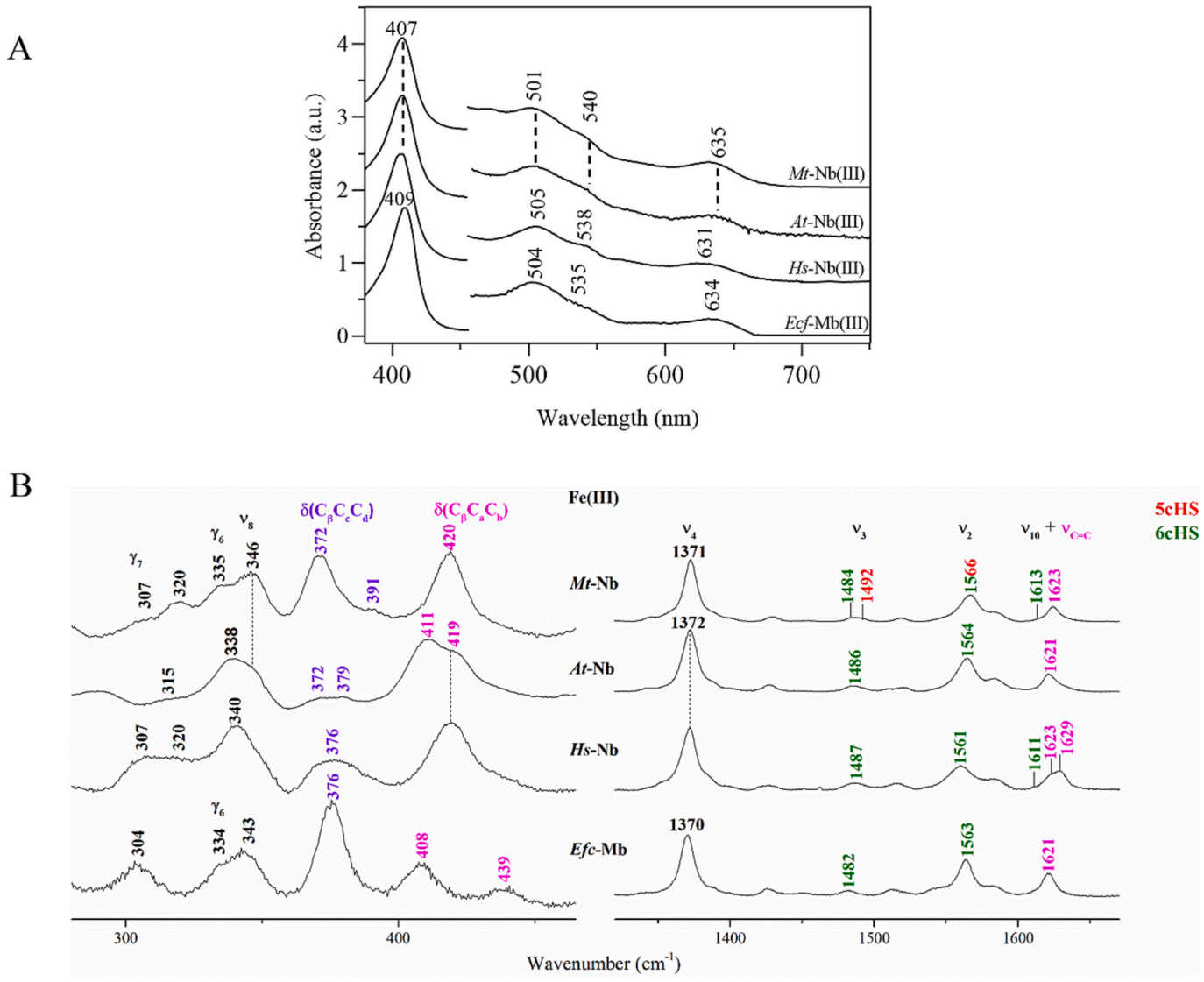

Fig. 2. UV–Vis (Panel A) and RR spectra of ferric *Mt*—Nb [33], *At*—Nb (present study), and *Hs*—Nb [33] obtained upon 406.7 nm excitation in the low (Panel B, *left side*) and high (Panel B, *right side*) wavenumber regions at about pH 6.0. The spectra of *Efc*-Mb in similar conditions are reported for comparison [43]. The bands characteristic of the 5cHS and 6cHS species are indicated in red and green, respectively, while the vibrational modes of the propionate and vinyl groups are displayed in purple and magenta, respectively. Experimental conditions for *At*-Nb(III): 5 mW at the sample, 75 min integration time. (For interpretation of the references to colour in this figure legend, the reader is referred to the web version of this article).

[33] and overlapped in a single band, approximately centered at 416–420 cm^{-1}, while in *At*-Nb(III) and in *Efc*-Mb(III) two $\delta(C_\beta C_a C_b)$ modes are observed at 411/419 cm^{-1} and 408/439 cm^{-1} [43,52], respectively. The propionate groups give rise to $\delta(C_\beta C_c C_d)$ in-plane bending modes characterized by two broad bands at 372 and 379 cm^{-1} in *At*-Nb(III) and centered at 376 cm^{-1} in *Hs*-Nb(III). Differently, in this wavenumber region *Mt*-Nb(III) displays a RR spectrum very similar to that of *Efc*-Mb(III) [43] and shows an intense $\delta(C_\beta C_c C_d)$ mode at 372 cm^{-1} with a shoulder at 391 cm^{-1} [43]. The different intensity and wavenumber of the propionate bending modes observed among the investigated Nbs suggest different H-bond interactions between the propionate and the surrounding amino acid residues of the protein pocket. In fact, the strength and number of hydrogen bonds between the propionate and polar amino acids in the heme cavity influences the propionate δ ($C_\beta C_c C_d$) bending modes wavenumbers, and stronger hydrogen bonds are correlated to higher wavenumbers [54–58].

3.2. Fe(II) forms

3.2.1. Unliganded Fe(II)

The RR high wavenumber spectra of ferrous *Mt*-Nb, *At*-Nb, and *Hs*-Nb and *Efc*-Mb (*i.e.*, *Mt*-Nb(II), *At*-Nb(II), *Hs*-Nb(II) and *Efc*-Mb(II), respectively) [34,50], show the typical pattern of pure 5cHS species as confirmed by the UV–Vis absorption spectra (Fig. 3, panels A and B).

In *Mt*-Nb(II), similarly to *Efc*-Mb(II), the vinyl stretching modes give rise to a single band at 1621 and 1618 cm^{-1}, respectively [34,52]. On the contrary, in *At*-Nb(II) and *Hs*-Nb(II) [34], two ν(C=C) modes are observed at 1621 and 1627 cm^{-1}, thus suggesting a different orientation of the two vinyl groups (Fig. 3, panel B). The corresponding $\delta(C_\beta C_a C_b)$ vinyl bending modes in *Mt*-Nb(II) and *Hs*-Nb(II) give rise to a broad band at 417 cm^{-1}, while in *At*-Nb(II) two bending modes are found at 410 and 417 cm^{-1}, analogously to what observed for the corresponding vinyl stretching modes (Fig. 3, panel B). Moreover, the $\delta(C_\beta C_c C_d)$ propionate in-plane bending modes give rise to a sharp band at 365 cm^{-1} with a shoulder at 377 cm^{-1} in *Mt*-Nb(II), and to a broad band at 365–375 cm^{-1} in *At*-Nb(II) and *Hs*-Nb(II), [34]. In *Efc*-Mb(II) the two propionates bending modes overlap giving rise to a very strong sharp band at 376 cm^{-1} [52].

In the low-frequency region of the spectrum, obtained with the 441.6 nm excitation line, an intense band was observed at 213 cm^{-1}, for *Mt*-Nb(II) and *Hs*-Nb(II) [34] (Fig. 3, panel B). Based on its intensity decrease upon excitation with the 413.1 nm (data not shown), it was assigned to the ν(Fe-His) stretching mode, which is expected to give rise to a strong band in 5cHS ferrous heme proteins upon excitation in the Soret band [49]. Usually, the ν(Fe-His) stretching mode frequency spans from about 200 cm^{-1} (neutral proximal His) to 250 cm^{-1} (deprotonated

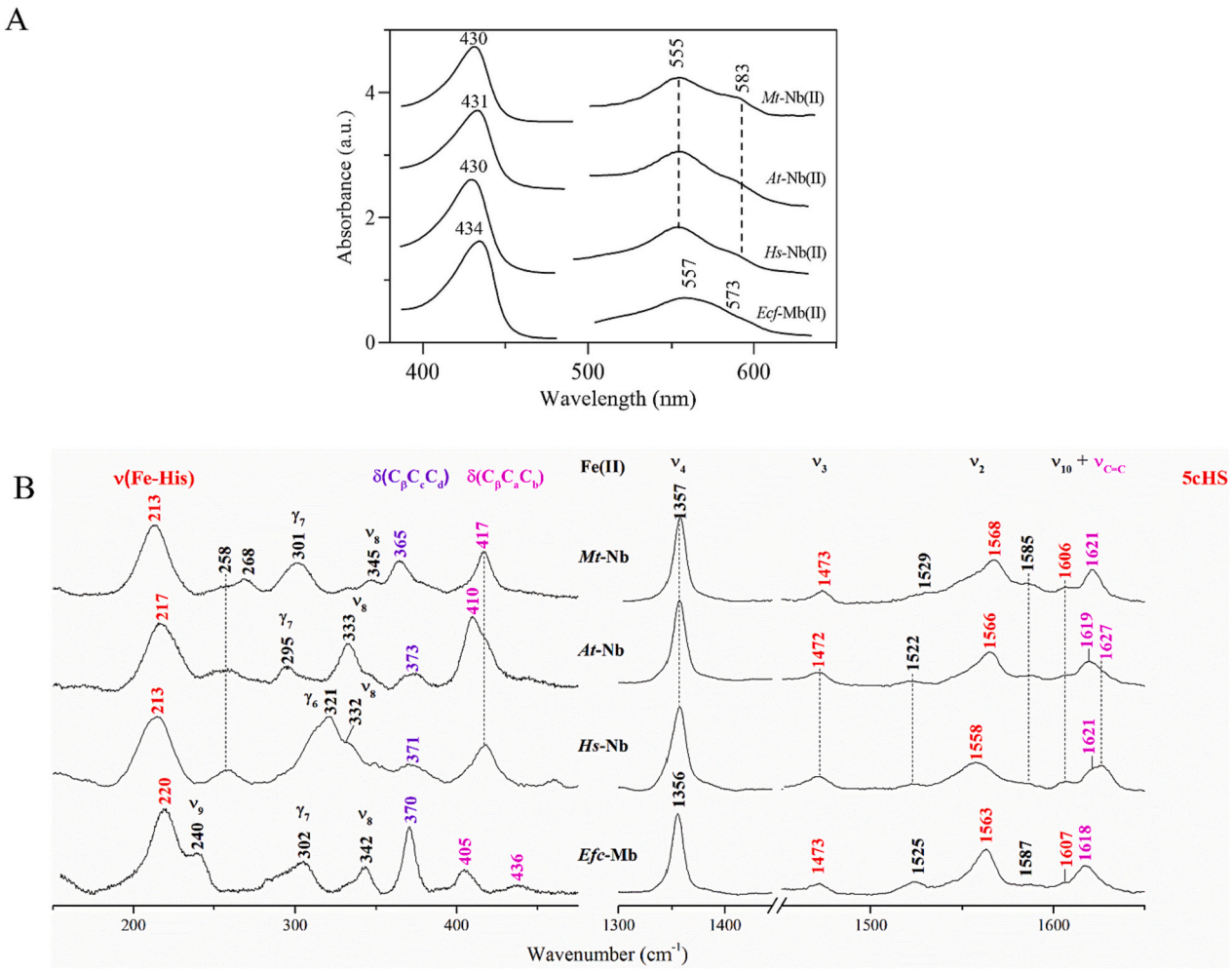

Fig. 3. UV–Vis (Panel A) and RR spectra of ferrous *Mt*—Nb, [34], *At*—Nb (present study), and *Hs*—Nb [34] obtained upon 441.6 nm excitation in the low (Panel B, *left side*) and high (Panel B, *right side*) wavenumber regions at pH 7.0. The spectra of *Efc*-Mb in similar conditions are reported for comparison [50,52]. The bands characteristic of the 5cHS and 6cLS species are indicated in red and blue, respectively, while the vibrational modes of the propionate and vinyl groups are displayed in purple and magenta, respectively. Experimental conditions for *At*-Nb(II): 6.5 mW at the sample, 120 min integration time. (For interpretation of the references to colour in this figure legend, the reader is referred to the web version of this article).

N_δ). Its frequency is an optimal probe of the proximal cavity structure [59]. In *Efc*-Mb(II) and ferrous Physeter catodon Mb (*Pc*-Mb(II)), where the N_δ proton is H-bonded to a neutral backbone carbonyl group, the ν(Fe-His) stretch was found at 220 cm^{-1} [47,50]. Therefore, in ferrous Nbs the lower ν(Fe-His) wavenumber indicates a weaker interaction than in Mb(II). Interestingly, in *At*-Nb(II) the ν(Fe-His) wavenumber (217 cm^{-1}) is close to that of Mb(II), suggesting a similar proximal ligand strength.

3.2.2. Fe(II)-CO

Upon CO binding, all the investigated Nbs(II) give rise to a 6cLS complex with UV–Vis absorption bands at 419–420, 537 and 568 nm (Fig. 4, panel A). The wavenumbers of the RR vibrational modes of the carbonylated *Mt*-Nb(II), *At*-Nb(II) and *Hs*-Nb(II) complexes (i.e., *Mt*-Nb (II)-CO, *At*-Nb(II)-CO and *Hs*-Nb(II)-CO complexes, respectively) are reported in Fig. 4 (panel B) and listed in Table S1. Nbs show a single CO conformer, characterized by ν(FeC) / ν(CO) couples at 510 / 1958 cm^{-1}, and 509 / 1950 cm^{-1} for *Mt*-Nb(II)-CO and *Hs*-Nb(II)-CO, respectively. In addition, in the present study, the ν(FeC) and ν(CO) stretching mode wavenumbers of the *At*-Nb(II)-CO complex (present study; see Supplementary Materials, Table S1) are found at 503 cm^{-1} and at 1958 cm^{-1}. The latter is in fair agreement with the value of 1959 cm^{-1} for the ν(CO) in *At*-Nb(II)-CO, as previously reported by FTIR spectroscopy [30]. Unlike Nbs, wild type *Pc*-Mb(II) binds CO into three different conformations, denoted A_0, A_1, and A_3. A_0 is predominant at acid pH, and the other two species dominate above pH 7.0, being A_1 the main conformer [60]. For *Efc*-Mb(II) only the A_1 species has been identified by RR [50], while two ν(CO) stretching have been observed in the IR spectrum [61].

CO binding is an excellent probe of the distal cavity of heme proteins, as the CO vibrations are sensitive to the molecular environment of the bound ligand [62]. Since the back-donation from the Fe dπ to the CO π^* orbitals depends on polar interactions, a strong hydrogen bond between the bound CO and the protein distal residues favors back-donation, with a strengthening of the Fe—C bond and a corresponding weakening of the CO bond [62]. An inverse linear correlation between the ν(FeC) and ν(CO) stretching mode wavenumbers was found for heme proteins and heme-model compounds containing a His residue as the fifth heme-Fe (II) ligand [62,63]. The ν(FeC)/ν(CO) position along the correlation line reflects the type and strength of distal polar interactions [62,63]. Moreover, CO complexes with a weak or absent proximal ligand are located above the histidine line, as a result of the variations in the donor strength of the trans-ligand [63].

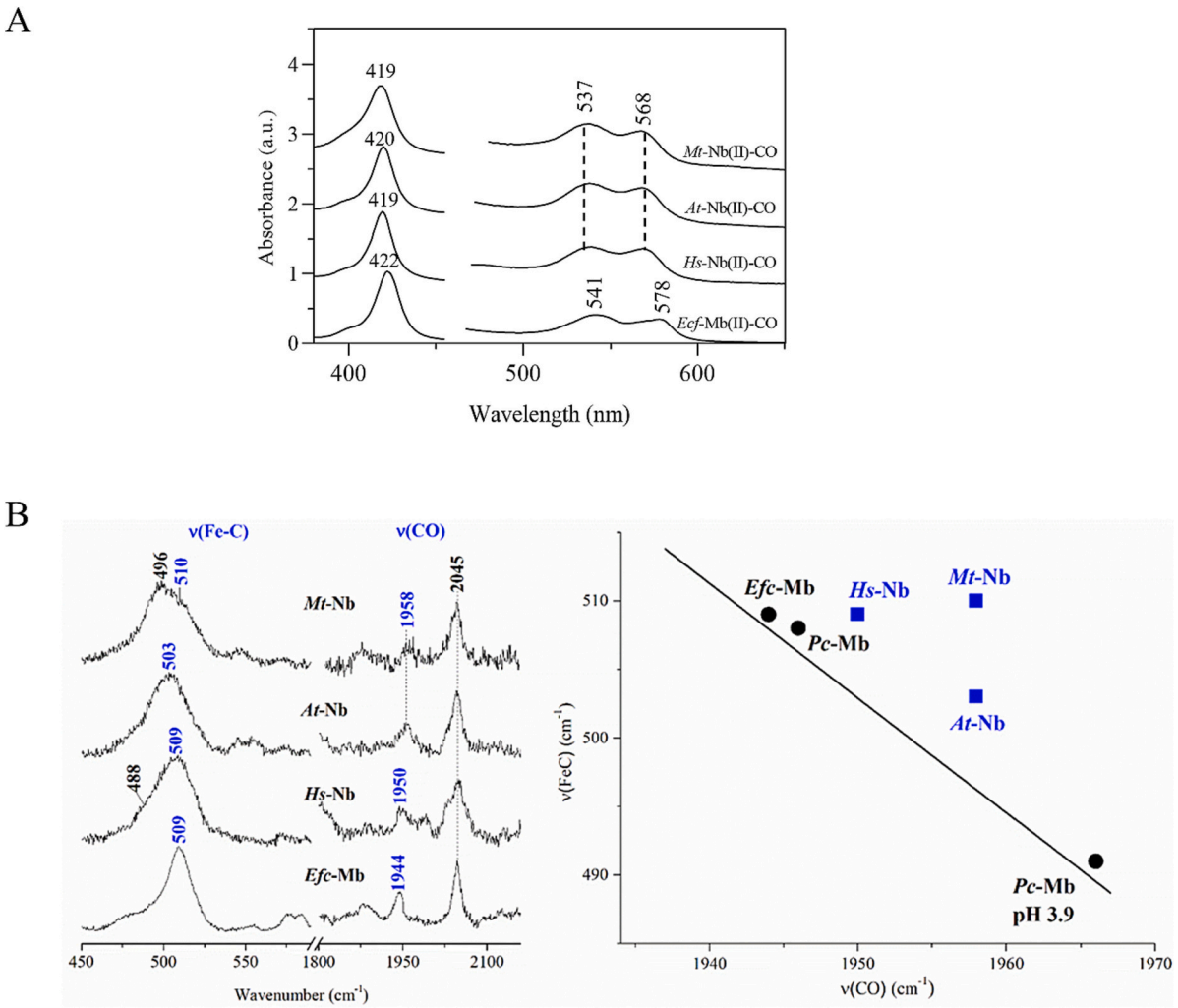

Fig. 4. UV–Vis (Panel A) and RR spectra (Panel B, *left side*) of *Mt*-Nb(II)-CO, [34], *At*-Nb(II)-CO (Table S1; present study), and *Hs*-Nb(II)-CO [34] obtained upon 413.1 nm laser line excitation in the 450–590 and 1800–2160 cm^{-1} wavenumber regions at pH 7.4. The spectra of *Efc*-Mb in similar conditions are reported for comparison [95]. Experimental conditions for *At*-Nb(II)-CO: 1.5 mW at the sample, 90 min integration time. (Panel B, *right* side) Back-bonding correlation plot of the ν(FeC) and ν(CO) stretching wavenumbers of the CO complexes of ferrous *Mt*—Nb, *At*—Nb, and *Hs*—Nb at pH 7.4 as obtained by RR spectroscopy (Panel B, *left side*). The corresponding wavenumbers of *Efc*-Mb at neutral pH, and *Pc*-Mb at neutral and acid pH [64], are reported for comparison. The solid line represents hexacoordinated carbonylated heme proteins with His as the proximal ligand. All the wavenumbers are listed in Table S1.

The ν(FeC)/ν(CO) points for all the investigated Nbs appear to be displaced above the histidine line, as shown in the Fig. 4, panel B, the effect being more pronounced for *Mt*-Nb(II)-CO with respect to *At*-Nb (II)-CO and *Hs*-Nb(II)-CO, as a consequence of a trans-ligand effect. In addition, the CO ligated form of *At*-Nb(II) shows a moderate back-bonding, weaker than that of *Hs*-Nb(II)-CO, indicating a slightly less polar cavity. This point appears also below the A_1 conformer of Mb, which is characterized by moderate back-bonding induced by weak H-bonding from the distal His residue (*Efc*-Mb(II)-CO: 509 and 1944 cm^{-1}; *Pc*-Mb(II)-CO: 508 and 1946 cm^{-1}) [50,64]. Mbs at acid pH [64] (*e.g.*, *Pc*-Mb at pH 3.9), similar to Mb variants where the distal His is replaced by non-polar residues [65], are characterized by ν(FeC) and ν(CO) modes at 491 and 1966 cm^{-1}, respectively, reflecting a decrease in back-bonding and thus an open cavity [63].

3.2.3. Fe(II)-NO

As shown in Fig. 5, the EPR spectra of nitrosylated *Mt*-Nb(II), *At*-Nb (II), *Hs*-Nb(II), and *Pc*-Mb(II) (i.e., *Mt*-Nb(II)-NO, *At*-Nb(II)-NO, *Hs*-Nb (II)-NO, and Pc-Mb(II)-NO, respectively) are very different. In fact, the EPR spectra of nitrosylated Nb(II) display the three-line hyperfine splitting constant of 17 G, which is absent in the EPR spectrum of *Efc*-Mb (II)-NO. This indicates a significant amount of cleavage of the heme-Fe (II)-His proximal bond of Nb(II)-NO already at pH 7.0, whereas the metal center of *Efc*-Mb(II)-NO is stably hexacoordinated under the same conditions [2,34,35,41,66–73].

4. Reactivity properties

4.1. Fe(II) derivative

Unlike *Pc*-Mb, Nbs display a rapid oxidation in the presence of O_2, envisaging a likely very low redox potential, even though no direct measurement has been carried out so far. As a result, the study of reduced Nb(II) forms can be undertaken only in the presence of a strong reductant like sodium dithionite, and precautions must be taken to prevent any exposure to gaseous phase and even minor O_2 contamination. Such a feature is reflected by the observation that values of the second-order rate constant of *Mt*-Nb(II), *At*-Nb(II), and *Hs*-Nb(II) oxidation by hydroxylamine ($1.1 \times 10^4\ M^{-1}\ s^{-1}$, $6.5 \times 10^4\ M^{-1}\ s^{-1}$, and $2.2 \times 10^4\ M^{-1}\ s^{-1}$, respectively) [74] are 50- and 300-fold higher than that of *Pc*-Mb(II) ($2.5 \times 10^2\ M^{-1}\ s^{-1}$) [75]. As a consequence, the reactivity of Nb(II) with O_2 is limited to measuring the O_2 dissociation rate constant using the O_2-pulse method [76]. Table 1 reports values for three Nbs and *Pc*-Mb, highlighting their close similarity to each other. Despite the reported differences in the structural arrangement of the distal side of the heme pocket, where Nbs have an open access to the bulk solvent while *Pc*-Mb (see above) has a distal barrier, the similarity in the O_2 dissociation rate constants suggests that Nbs have a value of the overall free energy barrier for O_2 dissociation similar to that observed in *Pc*-Mb. This barrier is estimated to be around 68 ± 2.6 kJ/mol. However, it is very likely that this is only an overall similarity, since the major contribution to O_2 binding in *Pc*-Mb, which occurs through H-bonding with the distal His residue, cannot be the same in Nbs, where no distal His is present. The characterization of the O_2 dissociation pathway in Nbs is rendered very difficult by the dramatic instability of the Nb(II)-O_2 form, which rapidly converts to Nb(III) at a rate faster than the dead time of the stopped-flow ($\sim$ 2 ms). As a result, only a small percentage of Nb(II)-O_2 can be observed by O_2 pulse experiments [33].

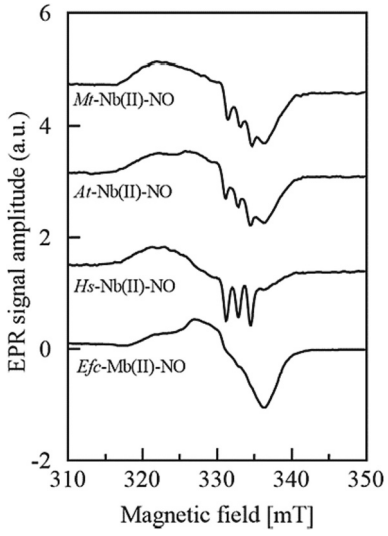

Fig. 5. EPR spectra of *Mt*-Nb(II)-NO, *At*-Nb(II)-NO, *Hs*-Nb(II)-NO and *Efc*-Mb (II)-NO at pH 7.0 and 110 K [34,41]. The percentage of the five-coordinated form of the heme-Fe(II) atom is 0.55 for *Mt*-Nb(II)-NO, 0.54 for *At*-Nb(II)-NO, 0.88 for *Hs*-Nb(II)-NO, and 0.00 for *Efc*-Mb(II)-NO [34,41].

The reactivity of Nb(II) towards CO and NO exhibits similarities when compared to *Pc*-Mb(II). The association rate constants values for CO and NO binding to Nb(II) are 2- to 5-fold and 10- to 30-fold lower, respectively, than those of *Pc*-Mb(II) (Table 1). However, when the reaction is monitored using stopped-flow, only a slow association rate constant is observed for both CO and NO binding to Nb(II) (Table 1). In contrast, laser photolysis experiments reveal a bimolecular biphasic rebinding process, with a minor fast phase displaying values similar to *Pc*-Mb(II) and a major slower phase showing values closer to those obtained by stopped-flow (Table 1). This feature might be tentatively explained by the shielding of the heme distal pocket from the bulk solvent, as reported for ligand-free *Mt*-Nb(III) [33], suggesting that a dense network of water molecules act as a barrier in Nbs, slowing down ligand binding during the rapid-mixing method. Since the very crowded network of water molecules is essentially dissipated upon binding of a diatomic ligand [33], the approximately 20-fold faster bimolecular rate constants observed by laser photolysis for CO and NO (Table 1) likely correspond to ligand rebinding before the reorganization of the water solvent network. According to this hypothesis, the fast rate likely corresponds to CO and NO rebinding preceding the formation of the water solvent network, whereas the slow rate, similar to that observed by rapid-mixing stopped-flow, possibly reflects ligand binding after the restoration of the water solvent network. This being the case, the free energy barrier represented by the water solvent network can be estimated to be 7.3 kJ/mol, and the rate constant for the reformation of the water solvent network after ligand dissociation should be $1000 \pm 500\ s^{-1}$.

An additional functional difference between Nbs(II) and *Pc*-Mb(II) is the pH effect on the proximal Fe(II)-His bond; thus, unliganded *Pc*-Mb (II) shows a cleavage (or a severe weakening) of the proximal bond at pH $\leq$ 3.5 with a consequent enhancement of the CO binding rate constant [77–79], whereas no evidence of a proton-linked cleavage has been observed for unliganded Nb(II), even at pH = 2.3, resulting in a pH-independence of the CO association velocity [34]. Such a feature would envisage either a stronger proximal Fe-His bond or a lower accessibility of bulk protons to the proximal His residue in Nbs than in *Pc*-Mb(II). This explanation seems more plausible to explain the pH-independent behavior of Nbs, considering their highly hydrophobic environment on the proximal side of the heme pocket [32]. In fact, the proximal Fe-His bond in Nbs is shielded from the bulk protons, leading to a significant decrease in the "apparent" pK_a for the protonation of the proximal histidyl side chain. The compactness and rigidity of the proximal pocket in Nbs might contribute to the weakening of the Fe-His bond when a ligand, such as CO and/or NO, is bound in the *trans*-axial position. Consequently, in these ligand-bound forms, the Fe-His bond of Nbs is either cleaved or significantly weakened. This unusual finding has been highlighted by EPR spectroscopy in Nb(II)-NO species [34,35] as well as by RR spectroscopy in Fe(II)-CO derivatives, and is supported by the fast CO dissociation rate constant (Figs. 4 and 5, and Table 1) [34].

Table 1
Values of kinetic and thermodynamic parameters for O_2, CO, and NO (*i.e.*, L) binding to ferrous nitrobindins and myoglobin (*i.e.*, Fe(II)).

Heme-protein	$k_{off(O2)}$ (s^{-1})	$k_{on(CO)}$ ($M^{-1}\,s^{-1}$)	$k_{off(CO)}$ (s^{-1})	$k_{off(CO)}/k_{on(CO)}$ (M)	$k_{on(NO)}$ (s^{-1})	$k_{off(NO)}$ ($M^{-1}\,s^{-1}$)	$k_{off(NO)}/k_{on(NO)}$ (M)
Mt-Nb(II) [a]	$(1.1 \pm 0.1) \times 10^1$	$(5.5 \pm 0.6) \times 10^4$ [b] $(1.6 \pm 0.3) \times 10^5$ (~40%) [c] $(8.3 \pm 1.0) \times 10^4$ (~60%) [c]	3.5 ± 0.5	$(6.3 \pm 0.6) \times 10^{-5}$	$(1.7 \pm 0.3) \times 10^6$ [b]	$(6.8 \pm 0.7) \times 10^{-2}$	$(4.0 \pm 0.5) \times 10^{-8}$
At-Nb(II)	6.8 ± 0.7 [a]	2.3×10^5 [b, d]	5.0×10^{-2} [d]	2.2×10^{-7} [d]	8.1×10^7 [b, d]	~8×10^{-3} [d]	~1×10^{-9} [d]
Hs-Nb(II) [a]	$(1.9 \pm 0.3) \times 10^1$	$(1.0 \pm 0.2) \times 10^5$ [b] $(3.9 \pm 0.5) \times 10^6$ (~15%) [c] $(1.7 \pm 0.3) \times 10^5$ (~85%) [c]	3.8 ± 0.5	$(3.8 \pm 0.4) \times 10^{-5}$	$(9.3 \pm 1.1) \times 10^5$ [b] $(1.5 \pm 0.3) \times 10^7$ (~12%) [c] $(8.5 \pm 1.0) \times 10^5$ (~88%) [c]	$(2.1 \pm 0.3) \times 10^{-3}$	$(2.3 \pm 0.5) \times 10^{-8}$
Pc-Mb(II)	1.0×10^1 [e]	5.1×10^5 [f]	1.9×10^{-2} [f]	3.7×10^{-8} [f]	2.2×10^7 [b, g]	1.2×10^{-4} [g, h]	5.5×10^{-12}

[a] pH 7.0; 25.0 °C. From [34].
[b] Determined by rapid-mixing stopped-flow.
[c] pH 7.0; 20.0 °C. The standard deviation was not available. From [30].
[d] pH 7.0; 20.0 °C. The standard deviation was not available. From [30].
[e] pH 7.0; 20.0 °C. The standard deviation was not available. From [92].
[f] pH 7.0; 20.0 °C. The standard deviation was not available. From [48].
[g] pH 7.0; 20.0 °C. The standard deviation was not available. From [96].
[h] pH 7.0; 20.0 °C. The standard deviation was not available. From [97].

4.2. Fe(III) derivative

As reported above, the most stable Nb form is the oxidized ferric Fe (III) species; this property is responsible for the peculiar behavior of the reaction of Nb(II)-NO with O_2 [39]. Unlike Mb(II)-NO, whose oxidation rate ($k_{autox} = (1.2 \pm 0.04) \times 10^{-4}\,s^{-1}$) is rate-limited by the dissociation of NO ($k_{off(NO)} = (1.2 \pm 0.3) \times 10^{-4}\,s^{-1}$) [80], O_2 oxidizes directly the Nb(II)-NO complexes. This reaction leads to the transient formation of the Nb(III)-N(*O*)O_2 species, which then dissociates to Nb(III) and NO_3^-. Values of the second-order rate constant for the formation of the Nb(III)-N(*O*)O_2 species range between $(1.4 \pm 0.2) \times 10^3\,M^{-1}\,s^{-1}$ and $(6.3 \pm 0.8) \times 10^3\,M^{-1}\,s^{-1}$ and values for the conversion of Nb(III)-N(*O*)O_2 to Nb(III) and NO_3^- are exceeding $5 \times 10^3\,s^{-1}$. Thus, the O_2-based oxidation of Nb(II)-NO is faster than the conversion of *Pc*-Mb(II)-NO to *Pc*-Mb(III) and NO_3^- [41].

Nb(III) interacts with NO displaying bimolecular association rate constants that are 15- to 30-fold faster than that of *Pc*-Mb(III) (Table 2) [36]. Moreover, values of kinetic parameters for NO binding to Nb(III) are closely similar to those observed for Nb(II)-NO complex formation (Table 1). Since the second-order rate constant for NO binding to *Pc*-Mb (II) is about 300-fold faster than for *Pc*-Mb(III) nitrosylation (Tables1 and 2), the close similarity of NO association to Nbs(III) and Nbs(II) is a very peculiar feature, indicating that the free energy barrier is essentially the same (*i.e.*, ~ 38.3 ± 1.0 kJ/mol). This behavior may be related to the similar shielding effect of the heme by the distal water molecules network [33]; therefore, the 1000-fold higher affinity of NO for Nb(II) than for Nb(III) reflects the 1000-fold difference of the first-order rate constant for NO dissociation from nitrosylated Nb(III) (Nb(III)-NO)) and Nb(II)-NO, due to the intrinsic features of the Fe(III)-NO and Fe(II)-NO bonds. Further, it is worth outlining that values of the NO dissociation rate constant for Nb(III)-NO are 10- to 20-fold faster than that for NO dissociation from *Pc*-Mb(III)-NO (Table 2) [36,39], while they are 200- to 700-fold faster for Nb(II)-NO with respect to nitrosylated *Pc*-Mb(III) (i.e., *Pc*-Mb(III)-NO) (Table 2) [30,36,39]. Such a behavior possibly reflects both (*i*) the dissipation of the water molecules network upon ligand binding, and (*ii*) the very open communication between the distal site of the heme pocket and the bulk solvent [33]. As a whole, while *Pc*-Mb(II)-NO appears to act as a NO trap, Nb(II)-NO appears as a NO storage (with a 10,000-fold lower affinity than in *Pc*-Mb(II)-NO) and Nb (III)-NO a potential signaling molecule as well as a NO source closely related to Nb(II)-NO. Interestingly, *Hs*—Nb represents the *C*-terminal domain of the nuclear protein THAP4, which has been postulated to act as a gas sensor able to modulate its transcriptional activity residing at the *N*-terminus [31,33,81].

As already reported for *Pc*-Mb [82], the Nb(III)-NO is shifted at pH ≥ 7.6 bringing about the OH^--induced reductive nitrosylation of Nb (III)-NO to Nb(II)-NO (Fig. S1); this process displays a rate constant 15- to 20-fold faster than that of *Pc*-Mb(III)-NO (Table 3). The fast conversion of Nb(III)-NO to Nb(II)-NO may reflect the open heme distal pocket of Nbs and thus the high accessibility of the anionic OH^- to the reaction center, which represents the rate-limiting step of the overall process (Table 3 and Fig. S1) [36,39].

A final comment is deserved about the peroxynitrite scavenging activity of ferric Nbs which display a behavior similar to that of *Pc*-Mb(III). In fact, values of the second-order rate constant for peroxynitrite detoxification from *Mt*-Nb(III), *At*-Nb(III), and *Hs*-Nb(III) ($(6.9 \pm 0.6) \times 10^4\,M^{-1}\,s^{-1}$, $(3.7 \pm 0.5) \times 10^4\,M^{-1}\,s^{-1}$, and $(3.4 \pm 0.4) \times 10^4\,M^{-1}\,s^{-1}$, respectively) [33,40] are only 2- to 4-fold higher than that of *Pc*-Mb(III) ($(1.6 \pm 0.1) \times 10^4\,M^{-1}\,s^{-1}$) [83]. This is likely due to the fact that peroxynitrite access to the active site is scarcely affected by the barrier, operating for other ligands, even though a small effect can be observed with a faster reactivity for the Nb metal center with respect to *Pc*-Mb(III) [42].

5. Conclusion and perspectives

Data here reported emphasize that structural differences between all-α-helical and all-β-barrel heme-proteins influence their reactivity

Table 2
Values of kinetic and thermodynamic parameters for NO binding to ferric nitrobindins and myoglobin (*i.e.*, Fe(III)).

Heme-protein	$k_{on(NO)}$ ($M^{-1}\,s^{-1}$)	$k_{off(NO)}$ (s^{-1})	$K_{(NO)}$ (M)	$k_{off(NO)}/k_{on(NO)}$ (M)
Mt-Nb(III) [a]	$(1.8 \pm 0.2) \times 10^6$	$(3.3 \pm 0.7) \times 10^1$	$(5.0 \pm 1.5) \times 10^{-5}$	$(1.8 \pm 0.2) \times 10^{-5}$
At-Nb(III) [b]	1.2×10^6	7.3×10^1	n.d.	6.1×10^{-5}
Hs-Nb(III) [a]	$(1.1 \pm 0.1) \times 10^6$	$(4.7 \pm 0.8) \times 10^1$	$(4.4 \pm 1.2) \times 10^{-5}$	$(4.3 \pm 1.2) \times 10^{-5}$
Pc-Mb(III) [c]	$(6.8 \pm 0.7) \times 10^4$	3.1 ± 0.3	$(3.8 \pm 0.5) \times 10^{-5}$	$(4.5 \pm 0.5) \times 10^{-5}$

n.d., not determined.
[a] pH 7.0; 20.0 °C. From [33].
[b] pH 7.0; 20.0 °C. The standard deviation was not available. From [30].
[c] pH 7.2; 20.0 °C. From [36].

Table 3
Values of kinetic parameters for reductive nitrosylation of ferric nitrobindins and myoglobin.

Heme-protein	pH	K (M)	k_{lim} (s^{-1})	k_{OH-} ($M^{-1}\,s^{-1}$)
Mt-Nb(III) [a]	7.8	$(5.7 \pm 0.6) \times 10^{-5}$	$(2.5 \pm 0.3) \times 10^{-3}$	$(4.9 \pm 0.5) \times 10^{3}$
	8.2	$(5.2 \pm 0.6) \times 10^{-5}$	$(8.1 \pm 0.9) \times 10^{-3}$	
	8.7	$(4.8 \pm 0.5) \times 10^{-5}$	$(2.4 \pm 0.3) \times 10^{-2}$	
	9.2	$(5.0 \pm 0.6) \times 10^{-5}$	$(7.8 \pm 0.9) \times 10^{-2}$	
At-Nb(III) [b]	7.7	$(5.3 \pm 0.6) \times 10^{-5}$	$(6.1 \pm 0.6) \times 10^{-3}$	$(8.1 \pm 0.9) \times 10^{3}$
	8.1	$(7.3 \pm 0.7) \times 10^{-5}$	$(1.4 \pm 0.2) \times 10^{-2}$	
	8.6	$(5.4 \pm 0.6) \times 10^{-5}$	$(3.2 \pm 0.4) \times 10^{-2}$	
	9.1	$(7.7 \pm 0.8) \times 10^{-5}$	$(1.0 \pm 0.1) \times 10^{-1}$	
Hs-Nb(III) [a]	8.0	$(4.4 \pm 0.5) \times 10^{-5}$	$(6.7 \pm 0.7) \times 10^{-3}$	$(6.9 \pm 0.7) \times 10^{3}$
	8.6	$(5.6 \pm 0.7) \times 10^{-5}$	$(2.8 \pm 0.3) \times 10^{-2}$	
	8.9	$(5.6 \pm 0.7) \times 10^{-5}$	$(5.3 \pm 0.6) \times 10^{-2}$	
	9.2	$(5.7 \pm 0.6) \times 10^{-5}$	$(1.1 \pm 0.2) \times 10^{-1}$	
Pc-Mb(III) [c]	8.3	$(1.0 \pm 0.1) \times 10^{-3}$	$(8.8 \pm 0.2) \times 10^{-4}$	$(3.2 \pm 0.2) \times 10^{2}$
	9.0	$(1.1 \pm 0.1) \times 10^{-3}$	$(3.6 \pm 0.1) \times 10^{-3}$	
	9.2	$(1.6 \pm 0.2) \times 10^{-3}$	$(5.0 \pm 0.2) \times 10^{-3}$	

[a] Determined at 20.0 °C. From [39].
[b] Determined at 20.0 °C. Present study.
[c] Determined at 20.0 °C. From [82].

towards exogenous ligands. The reduced reactivity of Nb(II) towards exogenous ligands, such as CO and NO, is likely attributed to two factors. First, the presence of crowded H_2O molecules at the heme distal side hinders ligand binding. Second, the highly hydrophobic nature of the heme proximal side creates a barrier for the coordinated movement of the proximal His-Fe(II) bond and the metal ion towards the heme plane upon ligand binding. The three-dimensional structures of Nb determined so far [30,31,33] indicate a weakening of the His-Fe proximal bond, that is 0.10–0.17 Å longer than that observed in *Pc*-Mb and *Efc*-Mb [84,85]; such bond length differences are meaningful given the high resolution (ranging from 1.79 Å to 1.36 Å) of the three-dimensional structures examined and envisage an enhanced strain on the proximal bond in Nbs. This proximal strain also leads to a severe weakening, and even the cleavage, of the His-Fe(II) proximal bond in the ligand-bound forms (*i.e.*, Nb(II)-CO and Nb(II)-NO), resulting in a markedly accelerated dissociation rate constants for CO. However, this is not true for NO dissociation, since the cleavage of the proximal bond, as occurring for the α-chains of human Hb(II)-NO in the T-state, brings about a slowing down for the rate of NO dissociation [86]; therefore, the observed faster rate constant for NO dissociation from Nb(II)-NO must be attributed instead to the more open distal heme pocket and the absence of a distal His. The drastically different regulation of ligand-induced conformational changes in Nbs, compared to other monomeric heme-proteins like mammalian Mbs, aligns with their likely different physiological role [33,40,41]. Notably, Nbs exhibit a redox-linked coordination change of the heme-Fe atom in response to variations in NO and O_2 levels, modulating the redox equilibrium. Thus, raising of NO concentration pushes the equilibrium in favor of the reduced Nb(II)-NO form (with a severe weakening, or even a cleavage, of the proximal His-Fe(II) bond), whereas the increase of O_2 levels shifts quickly the equilibrium in favor of the oxidized Nb(III) form, leading to the reformation of the proximal His-Fe(III) bond. This behavior envisages a metabolic signaling role of Nbs since sensing of O_2 and NO levels causes a redox-linked coordination change of the heme-Fe atom, which is then transmitted to the protein matrix. This function might be of the utmost importance in poorly oxygenated tissues like the retinas of the eyes, where a delicate balance between oxygenation and blood flow (regulated by NO) is crucial. Dysfunction in this balance can contribute to pathological conditions such as glaucoma and diabetic retinopathy [87,88].

As reported for other heme-proteins, Nb could play an important role in maintaining NO levels especially in the eyes of fish, which undergo high hydrostatic pressure under deep diving conditions [89]. This hypothesis is based on transcriptomic data [90,91] that indicate increased levels of Nb expression in zebrafish embryonic retinal pigment and tissues subjected to constant hypoxia. Future *in vivo* studies will be conducted to further explore the role of Nb, which has thus far been investigated *in vitro* using biochemical assays.

Author statement

Conceptualization: P. Ascenzi, M. Coletta. Investigation: A. Coletta, G. De Simone, A. di Masi, A. Pasquadibisceglie, F. Sebastiani. Data curation: P. Ascenzi, M. Coletta, G. Smulevich. Writing: P. Ascenzi, M. Coletta, G. Smulevich.

Declaration of Competing Interest

Authors declare no conflict of interest.

Data availability

Data will be made available on request.

Acknowledgements

The grants of Dipartimenti di Eccellenza, MIUR, Roma, Italy (Legge 232/2016, Art. 1, Comma 314-337; G.D.S., A.d.M., A.P., P.A) and Italian Ministry of Health and Fondazione Roma, Roma, Italy (M.C.).

Appendix A. Supplementary data

Supplementary data to this article can be found online at https://doi.org/10.1016/j.jinorgbio.2023.112387.

References

[1] E. Antonini, M. Brunori, Hemoglobin and Myoglobin in their Reactions with Ligands, North Holland Publishing Co., Amsterdam, 1971.
[2] M.F. Perutz, Regulation of oxygen affinity of hemoglobin: influence of structure of the globin on the heme iron, Annu. Rev. Biochem. 48 (1979) 327–386, https://doi.org/10.1146/annurev.bi.48.070179.001551.
[3] H.F. Bunn, B.G. Forget, Hemoglobin: Molecular, Genetic and Clinical Aspects, Saunders, W.B, Philadelphia, 1986.
[4] Ortiz de Montellano, P.R. *Cytochrome P450: Structure, Mechanism, and Biochemistry*, Plenum, New York, 1995.
[5] J.S. Olson, G.N. Phillips Jr., Kinetic pathways and barriers for ligand binding to myoglobin, J. Biol. Chem. 271 (1996) 17593–17596, https://doi.org/10.1074/jbc.271.30.17593.
[6] H.B. Gray, J.R. Winkler, Electron transfer in proteins, Annu. Rev. Biochem. 65 (1996) 537–561, https://doi.org/10.1146/annurev.bi.65.070196.002541.
[7] M. Bolognesi, D. Bordo, M. Rizzi, C. Tarricone, P. Ascenzi, Nonvertebrate hemoglobins: structural bases for reactivity, Prog. Biophys. Mol. Biol. 68 (1997) 29–68, https://doi.org/10.1016/s0079-6107(97)00017-5.
[8] K.R. Rodgers, Heme-based sensors in biological systems, Curr. Opin. Chem. Biol. 3 (1999) 158–167, https://doi.org/10.1016/S1367-5931(99)80028-3.

[9] M.K. Chan, Recent advances in heme-protein sensors, Curr. Opin. Chem. Biol. 5 (2001) 216–222, https://doi.org/10.1016/s1367-5931(00)00193-9.

[10] L.J. Smith, A. Kahraman, J.M. Thornton, Heme proteins–diversity in structural characteristics, function, and folding, Proteins 78 (2010) 2349–2368, https://doi.org/10.1002/prot.22747.

[11] H.M. Girvan, A.W. Munro, Heme sensor proteins, J. Biol. Chem. 288 (2013) 13194–13203, https://doi.org/10.1074/jbc.R112.422642.

[12] P. Ascenzi, M. Brunori, A molecule for all seasons: the heme, Journal of Porphyrins and Phthalocyanines 20 (2016) 16, https://doi.org/10.1142/S1088424616300081.

[13] W.R. Montfort, A. Weichsel, J.F. Andersen, Nitrophorins and related antihemostatic lipocalins from *Rhodnius prolixus* and other blood-sucking arthropods, Biochim. Biophys. Acta 1482 (2000) 110–118, https://doi.org/10.1016/s0167-4838(00)00165-5.

[14] J.F. Andersen, Structure and mechanism in salivary proteins from blood-feeding arthropods, Toxicon 56 (2010) 1120–1129, https://doi.org/10.1016/j.toxicon.2009.11.002.

[15] G. De Simone, P. Ascenzi, A. di Masi, F. Polticelli, Nitrophorins and nitrobindins: structure and function, Biomol. Concepts 8 (2017) 105–118, https://doi.org/10.1515/bmc-2017-0013.

[16] T. Takano, Structure of myoglobin refined at 2·0 Å resolution: I. crystallographic refinement of metmyoglobin from sperm whale, J. Mol. Biol. 110 (1977) 537–568, https://doi.org/10.1016/S0022-2836(77)80111-3.

[17] T. Takano, Structure of myoglobin refined at 2·0 Å resolution: II. Structure of deoxymyoglobin from sperm whale, J. Mol. Biol. 110 (1977) 569–584, https://doi.org/10.1016/S0022-2836(77)80112-5.

[18] M. Nardini, A. Pesce, M. Bolognesi, Truncated (2/2) hemoglobin: unconventional structures and functional roles *in vivo* and in human pathogenesis, Mol. Aspects Med. 84 (2022) 101049, https://doi.org/10.1016/j.mam.2021.101049.

[19] R.E. Dickerson, I. Geiss, The Structure and Action of Proteins, Harper and Row Publishers, New York, 1969.

[20] E. Domingues-Hamdi, C. Vasseur, J.B. Fournier, M.C. Marden, H. Wajcman, V. Baudin-Creuza, Role of α-globin H helix in the building of tetrameric human hemoglobin: interaction with α-hemoglobin stabilizing protein (AHSP) and heme molecule, PloS One 9 (2014), e111395, https://doi.org/10.1371/journal.pone.0111395.

[21] C. Vasseur, V. Baudin-Creuza, Role of α-hemoglobin molecular chaperone in the hemoglobin formation and clinical expression of some hemoglobinopathies, Transfus Clin Bio 22 (2015) 49–57, https://doi.org/10.1016/j.tracli.2015.01.002.

[22] T. Kitagawa, M.R. Ondrias, D.L. Rousseau, M. Ikeda-Saito, T. Yonetani, Evidence for hydrogen bonding of bound dioxygen to the distal histidine of oxycobalt myoglobin and haemoglobin, Nature 298 (1982) 869–871, https://doi.org/10.1038/298869a0.

[23] J.S. Olson, A.J. Mathews, R.J. Rohlfs, B.A. Springer, K.D. Egeberg, S.G. Sligar, J. Tame, J.P. Renaud, K. Nagai, The role of the distal histidine in myoglobin and haemoglobin, Nature 336 (1988) 265–266, https://doi.org/10.1038/336265a0.

[24] R.E. Brantley Jr., S.J. Smerdon, A.J. Wilkinson, E.W. Singleton, J.S. Olson, The mechanism of autooxidation of myoglobin, J. Biol. Chem. 268 (1993) 6995–7010.

[25] M. Becana, I. Yruela, G. Sarath, P. Catalan, M.S. Hargrove, Plant hemoglobins: a journey from unicellular green algae to vascular plants, New Phytol. 227 (2020) 1618–1635, https://doi.org/10.1111/nph.16444.

[26] H. Wajcman, L. Kiger, M.C. Marden, Structure and function evolution in the superfamily of globins, C. R. Biol. 332 (2009) 273–282, https://doi.org/10.1016/j.crvi.2008.07.026.

[27] T. Burmester, T. Hankeln, Function and evolution of vertebrate globins, Acta Physiol (Oxf.) 211 (2014) 501–514, https://doi.org/10.1111/apha.12312.

[28] H.J. Vreman, J.J. Mahoney, D.K. Stevenson, Carbon monoxide and carboxyhemoglobin, Adv. Pediatr. 42 (1995) 303–334.

[29] C. Bonaventura, A. Fago, R. Henkens, A.L. Crumbliss, Critical redox and allosteric aspects of nitric oxide interactions with hemoglobin, Antioxid. Redox Signal. 6 (2004) 979–991, https://doi.org/10.1089/ars.2004.6.979.

[30] C.M. Bianchetti, G.C. Blouin, E. Bitto, J.S. Olson, G.N. Phillips Jr., The structure and NO binding properties of the nitrophorin-like heme-binding protein from *Arabidopsis thaliana* gene locus At1g79260.1, Proteins 78 (2010) 917–931, https://doi.org/10.1002/prot.22617.

[31] C.M. Bianchetti, C.A. Bingman, G.N. Phillips Jr., Structure of the *C*-terminal heme-binding domain of THAP domain containing protein 4 from Homo sapiens, Proteins 79 (2011) 1337–1341, https://doi.org/10.1002/prot.22944.

[32] G. De Simone, P. Ascenzi, F. Polticelli, Nitrobindin: an ubiquitous family of all β-barrel heme-proteins, IUBMB Life 68 (2016) 423–428, https://doi.org/10.1002/iub.1500.

[33] G. De Simone, A. di Masi, G.M. Vita, F. Polticelli, A. Pesce, M. Nardini, M. Bolognesi, C. Ciaccio, M. Coletta, E.S. Turilli, et al., Mycobacterial and human nitrobindins: structure and function, Antioxid. Redox Signal. 33 (2020) 229–246, https://doi.org/10.1089/ars.2019.7874.

[34] G. De Simone, A. di Masi, A. Pesce, M. Bolognesi, C. Ciaccio, L. Tognaccini, G. Smulevich, S. Abbruzzetti, C. Viappiani, S. Bruno, et al., Mycobacterial and human ferrous nitrobindins: spectroscopic and reactivity properties, Int. J. Mol. Sci. 22 (2021), https://doi.org/10.3390/ijms22041674.

[35] G. De Simone, P. Fattibene, F. Sebastiani, G. Smulevich, M. Coletta, P. Ascenzi, Dissociation of the proximal his-Fe bond upon NO binding to ferrous zebrafish nitrobindin, J. Inorg. Biochem. 236 (2022) 111962, https://doi.org/10.1016/j.jinorgbio.2022.111962.

[36] G. De Simone, F. Sebastiani, G. Smulevich, M. Coletta, P. Ascenzi, Nitrosylation of ferric zebrafish nitrobindin: a spectroscopic, kinetic, and thermodynamic study, J. Inorg. Biochem. 237 (2022) 111996, https://doi.org/10.1016/j.jinorgbio.2022.111996.

[37] T.K. Shokhireva, R.E. Berry, H. Zhang, N.V. Shokhirev, F.A. Walker, Assignment of ferriheme resonances for high- and low-spin forms of nitrophorin 3 by H and C NMR spectroscopy and comparison to Nitrophorin 2: heme pocket structural similarities and differences, Inorganica Chim Acta 361 (2008) 925–940, https://doi.org/10.1016/j.ica.2007.05.044.

[38] M. Knipp, H. Ogata, G. Soavi, G. Cerullo, A. Allegri, S. Abbruzzetti, S. Bruno, C. Viappiani, A. Bidon-Chanal, F.J. Luque, Structure and dynamics of the membrane attaching nitric oxide transporter nitrophorin 7, F1000Res 4 (2015) 45, https://doi.org/10.12688/f1000research.6060.1.

[39] G. De Simone, A. di Masi, C. Ciaccio, M. Coletta, P. Ascenzi, NO scavenging through reductive nitrosylation of ferric *mycobacterium tuberculosis* and *Homo sapiens* nitrobindins, Int. J. Mol. Sci. 21 (2020), https://doi.org/10.3390/ijms21249395.

[40] G. De Simone, A. di Masi, F. Polticelli, P. Ascenzi, Human nitrobindin: the first example of an all-β-barrel ferric heme-protein that catalyzes peroxynitrite detoxification, FEBS Open Bio 8 (2018) 2002–2010, https://doi.org/10.1002/2211-5463.12534.

[41] G. De Simone, A. di Masi, P. Fattibene, C. Ciaccio, C. Platas-Iglesias, M. Coletta, A. Pesce, P. Ascenzi, Oxygen-mediated oxidation of ferrous nitrosylated nitrobindins, J. Inorg. Biochem. 224 (2021) 111579, https://doi.org/10.1016/j.jinorgbio.2021.111579.

[42] G. De Simone, A. Coletta, A. di Masi, M. Coletta, P. Ascenzi, The balancing of peroxynitrite detoxification between ferric heme-proteins and CO_2: the case of zebrafish nitrobindin, Antioxidants (Basel) (2022) 11, https://doi.org/10.3390/antiox11101932.

[43] G. De Sanctis, G. Petrella, C. Ciaccio, A. Feis, G. Smulevich, M. Coletta, A comparative study on axial coordination and ligand binding in ferric mini myoglobin and horse heart myoglobin, Biophys. J. 93 (2007) 2135–2142, https://doi.org/10.1529/biophysj.106.098764.

[44] R. Maurus, C.M. Overall, R. Bogumil, Y. Luo, A.G. Mauk, M. Smith, G.D. Brayer, A myoglobin variant with a polar substitution in a conserved hydrophobic cluster in the heme binding pocket, Biochim. Biophys. Acta 1341 (1997) 1–13, https://doi.org/10.1016/s0167-4838(97)00064-2.

[45] X. Zhao, K. Vyas, B.D. Nguyen, K. Rajarathnam, G.N. La Mar, T. Li, G.N. Phillips Jr., R.F. Eich, J.S. Olson, J. Ling, et al., A double mutant of sperm whale myoglobin mimics the structure and function of elephant myoglobin, J. Biol. Chem. 270 (1995) 20763–20774, https://doi.org/10.1074/jbc.270.35.20763.

[46] H. Frauenfelder, B.H. McMahon, P.W. Fenimore, Myoglobin: the hydrogen atom of biology and a paradigm of complexity, Proc. Natl. Acad. Sci. U. S. A. 100 (2003) 8615–8617, https://doi.org/10.1073/pnas.1633688100.

[47] T. Kitagawa, K. Nagai, M. Tsubaki, Assignment of the Fe-Nε (his F8) stretching band in the resonance Raman spectra of deoxy myoglobin, FEBS Lett. 104 (1979) 376–378, https://doi.org/10.1016/0014-5793(79)80856-x.

[48] R.J. Rohlfs, A.J. Mathews, T.E. Carver, J.S. Olson, B.A. Springer, K.D. Egeberg, S. G. Sligar, The effects of amino acid substitution at position E7 (residue 64) on the kinetics of ligand binding to sperm whale myoglobin, J. Biol. Chem. 265 (1990) 3168–3176.

[49] T.G. Spiro, X.Y. Li, Biological Applications of Raman Spectroscopy, John Wiley & Sons Inc, New York, NY, USA, 1988.

[50] G. Smulevich, A.R. Mantini, M. Paoli, M. Coletta, G. Geraci, Resonance Raman studies of the heme active site of the homodimeric myoglobin from *Nassa mutabilis*: a peculiar case, Biochemistry 34 (1995) 7507–7516, https://doi.org/10.1021/bi00022a026.

[51] F. Sebastiani, A. Dali, G. Smulevich, The combination of resonance Raman spectroscopy and site directed mutagenesis to study the diverse aspects of heme protein structure and function, J. Porphyrins Phthalocyanines 26 (2022) 755–764.

[52] S. Hu, K.M. Smith, T.G. Spiro, Assignment of protoheme resonance raman spectrum by heme labeling in myoglobin, J. Am. Chem. Soc. 118 (1996) 12638–12646, https://doi.org/10.1021/ja962239e.

[53] M.P. Marzocchi, G. Smulevich, Relationship between heme vinyl conformation and the protein matrix in peroxidases, J. Raman Spectrosc. 34 (2003) 725–736, https://doi.org/10.1002/jrs.1037.

[54] D.S. Gottfried, E.S. Peterson, A. Sheikh, J. Wang, J.M. Friedman, Evidence for damped hemoglobin dynamics in a room temperature trehalose glass, J. Phys. Chem. 100 (1996) 12034–12042, https://doi.org/10.1021/jp9609489.

[55] E.S. Peterson, J.M. Friedman, E.Y. Chien, S.G. Sligar, Functional implications of the proximal hydrogen-bonding network in myoglobin: a resonance Raman and kinetic study of Leu89, Ser92, His97, and F-helix swap mutants, Biochemistry 37 (1998) 12301–12319, https://doi.org/10.1021/bi980752u.

[56] T. Gabler, F. Sebastiani, J. Helm, A. Dali, C. Obinger, P.G. Furtmuller, G. Smulevich, S. Hofbauer, Substrate specificity and complex stability of coproporphyrin ferrochelatase is governed by hydrogen-bonding interactions of the four propionate groups, FEBS J. 289 (2022) 1680–1699, https://doi.org/10.1111/febs.16257.

[57] A. Dali, T. Gabler, F. Sebastiani, A. Destinger, P.G. Furtmuller, V. Pfanzagl, M. Becucci, G. Smulevich, S. Hofbauer, Active site architecture of coproporphyrin ferrochelatase with its physiological substrate coproporphyrin III: propionate interactions and porphyrin core deformation, Protein Sci. 32 (2023), e4534, https://doi.org/10.1002/pro.4534.

[58] F. Sebastiani, C. Baroni, G. Patil, A. Dali, M. Becucci, S. Hofbauer, G. Smulevich, The role of the hydrogen bond network in maintaining heme pocket stability and protein function specificity of *C. diphtheriae* coproheme decarboxylase, Biomolecules (2023) 13, https://doi.org/10.3390/biom13020235.

[59] G. Smulevich, A. Feis, B.D. Howes, A. Ivancich, Structure-function relationships among heme peroxidases: new insights from electronic absorption, resonance Raman and multifrequency Electron paramagnetic resonance spectroscopies, in: K. M. Kadish, K.M. Smith, R. Guilard (Eds.), Handbook of Porphyrin Science with Applications to Chemistry, Physics, Materials Science, Engineering, Biology and Medicine, NMR and EPR Techniques, vol. 6, World Scientific, Singapore, 2010, pp. 367–455.
[60] J.D. Muller, B.H. McMahon, E.Y. Chien, S.G. Sligar, G.U. Nienhaus, Connection between the taxonomic substates and protonation of histidines 64 and 97 in carbonmonoxy myoglobin, Biophys. J. 77 (1999) 1036–1051, https://doi.org/10.1016/s0006-3495(99)76954-7.
[61] S. Nagao, H. Ishikawa, T. Yamada, Y. Mizutani, S. Hirota, Carbon monoxide binding properties of domain-swapped dimeric myoglobin, J. Biol. Inorg. Chem. 20 (2015) 523–530, https://doi.org/10.1007/s00775-014-1236-0.
[62] T.G. Spiro, I.H. Wasbotten, CO as a vibrational probe of heme protein active sites, J. Inorg. Biochem. 99 (2005) 34–44, https://doi.org/10.1016/j.jinorgbio.2004.09.026.
[63] K.M. Vogel, P.M. Kozlowski, M.Z. Zgierski, T.G. Spiro, Role of the axial ligand in heme CO backbonding; DFT analysis of vibrational data, Inorg. Chim. Acta 297 (2000) 11–17, https://doi.org/10.1016/S0020-1693(99)00253-4.
[64] D. Morikis, P.M. Champion, B.A. Springer, S.G. Sligar, Resonance raman investigations of site-directed mutants of myoglobin: effects of distal histidine replacement, Biochemistry 28 (1989) 4791–4800, https://doi.org/10.1021/bi00437a041.
[65] G.N. Phillips, M.L. Teodoro, T. Li, B. Smith, J.S. Olson, Bound CO is a molecular probe of electrostatic potential in the distal pocket of myoglobin, J. Phys. Chem. B. 103 (1999) 8817–8829, https://doi.org/10.1021/jp9918205.
[66] B.B. Wayland, L.W. Olson, Spectroscopic studies and bonding model for nitric oxide complexes of iron porphyrins, J. Am. Chem. Soc. 96 (1974) 6037–6041, https://doi.org/10.1021/ja00826a013.
[67] A. Szabo, M.F. Perutz, Equilibrium between six- and five-coordinated hemes in nitrosylhemoglobin: interpretation of electron spin resonance spectra, Biochemistry 15 (1976) 4427–4428, https://doi.org/10.1021/bi00665a013.
[68] R.W. Romberg, R.J. Kassner, Nitric oxide and carbon monoxide equilibria of horse myoglobin and (*N*-methylimidazole)protoheme. Evidence for steric interaction with the distal residues, Biochemistry 18 (1979) 5387–5392, https://doi.org/10.1021/bi00591a020.
[69] P. Ascenzi, G.M. Giacometti, E. Antonini, G. Rotilio, M. Brunori, Equilibrium and kinetic evidence for a transition between six- and five-coordinate ferrous heme in the nitric oxide derivative of Aplysia myoglobin, J. Biol. Chem. 256 (1981) 5383–5386.
[70] W.E. Blumberg, The study of hemoglobin by electron paramagnetic resonance spectroscopy, Methods Enzymol. 76 (1981) 312–329, https://doi.org/10.1016/0076-6879(81)76129-9.
[71] A.F. Duprat, T.G. Traylor, G.Z. Wu, M. Coletta, V.S. Sharma, K.N. Walda, D. Magde, Myoglobin-NO at low pH: free four-coordinated heme in the protein pocket, Biochemistry 34 (1995) 2634–2644, https://doi.org/10.1021/bi00008a030.
[72] B.P. Luchsinger, E.D. Walter, L.J. Lee, J.S. Stamler, D.J. Singel, EPR Studies of the Chemical Dynamics of NO and Hemoglobin. In High Resolution EPR: Applications to Metalloenzymes and Metals in Medicine, Springer, New York, NY, USA, 2009.
[73] S. Van Doorslaer, Probing the structure–function relationship of heme proteins using multifrequency pulse EPR techniques, in: L. Berliner, G. Hanson (Eds.), High Resolution EPR. Biological Magnetic Resonanc vol. 28, Springer, New York, NY, USA, 2009.
[74] G. De Simone, G.R. Tundo, A. Coletta, M. Coletta, P. Ascenzi, Hydroxylamine-induced oxidation of ferrous nitrobindins, J. Biol. Inorg. Chem. 27 (2022) 443–453, https://doi.org/10.1007/s00775-022-01940-9.
[75] R. Sturms, A.A. DiSpirito, D.B. Fulton, M.S. Hargrove, Hydroxylamine reduction to ammonium by plant and cyanobacterial hemoglobins, Biochemistry 50 (2011) 10829–10835, https://doi.org/10.1021/bi201425f.
[76] Q.H. Gibson, The contribution of the alpha and beta chains to the kinetics of oxygen binding to and dissociation from hemoglobin, Proc. Natl. Acad. Sci. U. S. A. 70 (1973) 1–4, https://doi.org/10.1073/pnas.70.1.1.
[77] G.M. Giacometti, T.G. Traylor, P. Ascenzi, M. Brunori, E. Antonini, Reactivity of ferrous myoglobin at low pH, J. Biol. Chem. 252 (1977) 7447–7448.
[78] T.G. Traylor, L.A. Deardurff, M. Coletta, P. Ascenzi, E. Antonini, M. Brunori, Reactivity of ferrous heme proteins at low pH, J. Biol. Chem. 258 (1983) 12147–12148, https://doi.org/10.1016/S0021-9258(17)44148-2.
[79] M. Coletta, P. Ascenzi, T.G. Traylor, M. Brunori, Kinetics of carbon monoxide binding to monomeric hemoproteins. Role of the proximal histidine, J. Biol. Chem. 260 (1985) 4151–4155.
[80] E.L. Foley, A.N. Hvitved, R.F. Eich, J.S. Olson, Mechanisms of nitric oxide reactions with globins using mammalian myoglobin as a model system, J. Inorg. Biochem. 233 (2022) 111839, https://doi.org/10.1016/j.jinorgbio.2022.111839.
[81] H.M. Sanghavi, S.S. Mallajosyula, S. Majumdar, Classification of the human THAP protein family identifies an evolutionarily conserved coiled coil region, BMC Struct. Biol. 19 (2019) 4, https://doi.org/10.1186/s12900-019-0102-2.
[82] M. Hoshino, M. Maeda, R. Konishi, H. Seki, P.C. Ford, Studies on the reaction mechanism for reductive nitrosylation of ferrihemoproteins in buffer solutions, J. Am. Chem. Soc. 118 (1996) 5702–5707, https://doi.org/10.1021/ja953311w.
[83] S. Herold, S. Kalinga, T. Matsui, Y. Watanabe, Mechanistic studies of the isomerization of peroxynitrite to nitrate catalyzed by distal histidine metmyoglobin mutants, J. Am. Chem. Soc. 126 (2004) 6945–6955, https://doi.org/10.1021/ja0493300.
[84] T.Y. Teng, V. Srajer, K. Moffat, Photolysis-induced structural changes in single crystals of carbonmonoxy myoglobin at 40 K, Nat. Struct. Biol. 1 (1994) 701–705, https://doi.org/10.1038/nsb1094-701.
[85] K. Chu, J. Vojtchovsky, B.H. McMahon, R.M. Sweet, J. Berendzen, I. Schlichting, Structure of a ligand-binding intermediate in wild-type carbonmonoxy myoglobin, Nature 403 (2000) 921–923, https://doi.org/10.1038/35002641.
[86] F. Azizi, J.E. Kielbasa, A.M. Adeyiga, R.D. Maree, M. Frazier, M. Yakubu, H. Shields, S.B. King, D.B. Kim-Shapiro, Rates of nitric oxide dissociation from hemoglobin, Free Radic. Biol. Med. 39 (2005) 145–151, https://doi.org/10.1016/j.freeradbiomed.2005.03.001.
[87] D.Y. Yu, S.J. Cringle, P.K. Yu, C. Balaratnasingam, A. Mehnert, M.V. Sarunic, D. An, E.N. Su, Retinal capillary perfusion: spatial and temporal heterogeneity, Prog. Retin. Eye Res. 70 (2019) 23–54, https://doi.org/10.1016/j.preteyeres.2019.01.001.
[88] S.S. Tummanapalli, R. Kuppusamy, J.H. Yeo, N. Kumar, E.J. New, M.D.P. Willcox, The role of nitric oxide in ocular surface physiology and pathophysiology, Ocul. Surf. 21 (2021) 37–51, https://doi.org/10.1016/j.jtos.2021.04.007.
[89] C. Damsgaard, Physiology and evolution of oxygen secreting mechanism in the fisheye, Comp. Biochem. Physiol. A Mol. Integr. Physiol. 252 (2021) 110840, https://doi.org/10.1016/j.cbpa.2020.110840.
[90] D.G. Howe, S. Ramachandran, Y.M. Bradford, D. Fashena, S. Toro, A. Eagle, K. Frazer, P. Kalita, P. Mani, R. Martin, et al., The zebrafish information network: major gene page and home page updates, Nucleic Acids Res. 49 (2021) D1058–D1064, https://doi.org/10.1093/nar/gkaa1010.
[91] C.E. Van Slyke, Y.M. Bradford, D.G. Howe, D.S. Fashena, S. Ramachandran, L. Ruzicka, Staff, Z, Z.F.I.N. Using, Data types, organization, and retrieval, Methods Mol. Biol. 2018 (1757) 307–347, https://doi.org/10.1007/978-1-4939-7737-6_11.
[92] M. Brunori, T.M. Schuster, Kinetic studies of ligand binding to hemoglobin and its isolated subunits by the temperature jump relaxation method, J. Biol. Chem. 244 (1969) 4046–4053, https://doi.org/10.1016/S0021-9258(17)36383-4.
[93] S.V. Evans, G.D. Brayer, High-resolution study of the three-dimensional structure of horse heart metmyoglobin, J. Mol. Biol. 213 (1990) 885–897, https://doi.org/10.1016/S0022-2836(05)80270-0.
[94] E.F. Pettersen, T.D. Goddard, C.C. Huang, G.S. Couch, D.M. Greenblatt, E.C. Meng, T.E. Ferrin, UCSF chimera–a visualization system for exploratory research and analysis, J. Comput. Chem. 2004 (1605-1612) 25, https://doi.org/10.1002/jcc.20084.
[95] L. Milazzo, S. Hofbauer, B.D. Howes, T. Gabler, P.G. Furtmuller, C. Obinger, G. Smulevich, Insights into the active site of coproheme decarboxylase from *listeria monocytogenes*, Biochemistry 57 (2018) 2044–2057, https://doi.org/10.1021/acs.biochem.8b00186.
[96] R.F. Eich, T. Li, D.D. Lemon, D.H. Doherty, S.R. Curry, J.F. Aitken, A.J. Mathews, K. A. Johnson, R.D. Smith, G.N. Phillips, J.S. Olson, Mechanism of NO-induced oxidation of myoglobin and hemoglobin, Biochemistry 35 (1996) 6976–6983, https://doi.org/10.1021/bi960442g.
[97] E.G. Moore, Q.H. Gibson, Cooperativity in the dissociation of nitric oxide from hemoglobin, J. Biol. Chem. 251 (1976) 2788–2794.